Microscopic theory of the proximity effect in superconductor-graphene nanostructures

P. Burset, A. Levy Yeyati, and A. Martín-Rodero
Departamento de Física Teórica de la Materia Condensada C-V, Universidad Autónoma de Madrid, E-28049 Madrid, Spain
(Received 11 February 2008; revised manuscript received 18 April 2008; published 19 May 2008)

We present a theoretical analysis of the proximity effect at a graphene-superconductor interface. We use a tight-binding model for the electronic states in this system, which allows us to describe the interface at the microscopic level. Two different interface models are proposed: one in which the superconductor induces a finite pairing in the graphene regions underneath, thus maintaining the honeycomb structure at the interface and one that assumes that the graphene layer is directly coupled to a bulk superconducting electrode. We show that properties such as the Andreev reflection probability and its channel decomposition critically depend on the model used to describe the interface. We also study the proximity effect on the local density of states on the graphene. For finite layers, we analyze the induced *minigap* and how it is reduced when the length of the layer increases. The results for the local density of states profiles for finite and semi-infinite layers are presented.

DOI: 10.1103/PhysRevB.77.205425 PACS number(s): 73.23.−b, 74.45.+c, 74.78.Na, 73.20.−r

I. INTRODUCTION

The possibility to isolate and perform direct transport measurements on few or even single graphite layers[1] has triggered a large activity in the condensed matter community. The case of a single layer of carbon atoms, known as graphene, is of particular interest because of its unique electronic structure, which, under certain conditions, corresponds to massless Dirac fermions confined in two dimensions.[2]

On the other hand, the coupling to a superconductor provides an interesting way to test the electronic properties of graphene. In a recent work of Beenakker,[3] it was shown that for an ideal interface between a superconductor and graphene, an unusual type of Andreev reflection, in which the hole is specularly reflected, appears. Several other effects involving graphene and superconductors such as Josephson transport,[4,5] re-entrance effect,[6] and quasiparticle transport mediated by multiple Andreev processes[7] have been theoretically analyzed.

In addition to its effect on the transport properties, the coupling to a superconductor should also produce a change in the electronic spectral properties and the induction of pairing correlations due to the proximity effect. The recent experimental achievement of good contact between superconducting electrodes and graphene layers[8] open the possibility to explore the proximity effect on these systems with great detail. Furthermore, experiments where the proximity effect on graphene could be explored even with atomic scale resolution by using scanning tunneling microscopy are underway.[9] At present, only the results for the total density of states (DOS) in superconductor-graphene-superconductor structures have been presented.[10]

The present work is aimed to study in detail the interface between the superconductor and the graphene sheet. To this end, we shall describe the electronic structure of graphene at the level of the tight-binding approximation. This description allows us to more microscopically analyze the superconductor-graphene interface as compared to a description where the continuous limit leading to an effective Dirac–Bogoliubov–de Gennes equation is taken from the start.[11] In the continuous description, it is usually assumed that the presence of the interface do not couple different valleys of the graphene band structure, which could not be the case in an actual experimental situation. Moreover, when the study is focused on finite size graphene sheets, a strong dependence on the geometry of the edges appears.[12] Thus, different symmetry directions will have distinct behavior.[13] For *zigzag* edges, zero-energy surface states appear,[13] which could hide the effects of the coupling to a superconductor.

In this work, we will concentrate on interfaces defined along an *armchair* edge. We propose two different models for this interface: The first one assumes that graphene is directly coupled to a bulk superconducting electrode, which does not maintain the honeycomb structure of the graphene sheet; the second model studies the possibility that one superconducting electrode on top of the graphene sheet induces a finite pairing amplitude and shifts the Fermi level of the graphene sheet far away from the Dirac point. As we discuss below, the two models lead to different behavior of the Andreev reflection probability as a function of energy, wave vector, and doping level. We further analyze several aspects of the spectral properties of the graphene layer within the two models both for the finite and the semi-infinite case.

The rest of the paper is organized as follows: In Sec. II, we introduce the tight-binding model for a graphene layer and we show the analytic expressions for the Green's functions for a semi-infinite and a finite layer. In Sec. III, the two different models for the interface with a superconductor are defined and a general expression for the self-energy, which provides the basis for the calculations of the following sections, is obtained. In Sec. IV, we study the model dependence of the Andreev reflection processes. In Sec. V, we also study the influence of the different interface models on the local density of states (LDOS) of a finite graphene layer coupled to a superconductor, analyzing in particular the minigap, which is induced in the case of metallic layers. Results for the spatially resolved DOS for a semi-infinite graphene layer are presented in Sec. VI. The paper is closed with some concluding remarks.

II. DESCRIPTION OF ISOLATED GRAPHENE LAYERS

For the description of the electronic states in a defect free graphene layer, we shall adopt the tight-binding approxima-

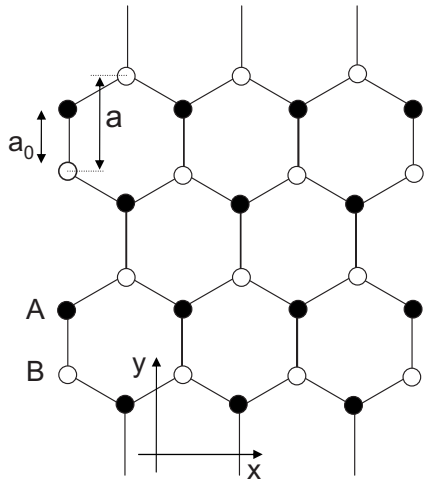

FIG. 1. The honeycomb structure of a graphene sheet is formed by combining two triangular sublattices, which are denoted by A (dots) and B (open dots). The unit cell on each horizontal line includes one atom from each sublattice. The axis selection used in this work is indicated.

tion, i.e., we use a model Hamiltonian of the type $\hat{H} = t_g \Sigma_{\langle ij\rangle,\sigma} \hat{c}^{\dagger}_{i\sigma} \hat{c}_{j\sigma} + \epsilon \Sigma_{i\sigma} \hat{c}^{\dagger}_{i\sigma} \hat{c}_{i\sigma}$, where t_g denotes the hopping element between nearest-neighbor carbon atoms on the honeycomb lattice and ϵ is a uniform site energy level, which allows to vary the level of doping ($\epsilon=0$ corresponds to the undoped case). The dispersion relation for the translational invariant case is given by $E(k,q) = \epsilon \pm t_g |1 + 2e^{iqa} \cos(ka/\sqrt{3})|$, where k and q denote the wave vector in the x and y directions, respectively, and a is the defined lattice parameter, as shown in Fig. 1 (as can be seen, $a = 3a_0/2$, where a_0 is the interatomic distance). For the undoped case, the Fermi surface collapses into two nonequivalent points at the Brillouin zone corresponding to $(k,q) = (\pm 2\pi/\sqrt{3}a, 0)$. The dispersion relation close to these points can be linearized with a slope $t_g a$, which fixes the Fermi velocity v_F.

A. Green's functions for a semi-infinite armchair graphene layer

We concentrate here in the derivation of the edge Green's function for a semi-infinite graphene layer with armchair orientation. We assume that there is a translational symmetry in the direction parallel to the edge (y). The semi-infinite system can be decomposed into lines of sites in the y direction, which are coupled by hopping elements with the neighboring lines on the x direction. The unit cell on each line includes two sites, corresponding to each triangular sublattice, that are denoted by A and B (see Fig. 1). These sites are coupled by a hopping element t_g within the unit cell. Thus, the cell Hamiltonian is given by

$$\hat{h} = \begin{pmatrix} \epsilon & t_g \\ t_g & \epsilon \end{pmatrix}.$$

The hopping elements between neighboring lines also couple sites of type A with sites of type B but should include a phase factor $e^{\pm iqa}$ due to the displacement of the cells in the y direction. The hopping matrix in the A-B space (both in the forward and in the backward directions) can be written as $\hat{t}(q) = t_g \hat{U}(q)$, where

$$\hat{U}(q) = \begin{pmatrix} 0 & e^{iqa} \\ e^{-iqa} & 0 \end{pmatrix}.$$

The self-similarity of the semi-infinite system with one additional line of sites leads to the following implicit equation for the edge Green's function:

$$\hat{g}(q,\omega) = [\omega \hat{I} - \hat{h} - t_g^2 \hat{U}(q) \hat{g}(q,\omega) \hat{U}(q)]^{-1}.$$

Hereafter, we implicitly assume that ω stands for $\omega \pm i\eta$ and that the limit $\eta \to 0$ is taken to obtain the retarded or the advanced component, respectively. We can now define $\hat{\tilde{g}} = \hat{U}\hat{g}$, which satisfies the simpler equation,

$$\hat{\tilde{g}} = [\hat{X}(q,\omega) - t_g^2 \hat{\tilde{g}}]^{-1},$$

where $\hat{X}(q,\omega) = (\omega \hat{I} - \hat{h})\hat{U}(q)$.

To obtain an explicit expression for $\hat{\tilde{g}}$, it is useful to perform a basis rotation in order to diagonalize the matrix $\hat{X}$. The general form of this rotation is $\hat{R} = \hat{R}_1 \hat{R}_2$, where $\hat{R}_1 = e^{iqa/2\hat{\sigma}_z}$, $\hat{\sigma}_z$ is the z Pauli matrix acting on the sublattice space, and

$$\hat{R}_2 = \frac{1}{\sqrt{-2\sin\alpha}} \begin{pmatrix} e^{i\alpha/2} & e^{-i\alpha/2} \\ ie^{-i\alpha/2} & ie^{i\alpha/2} \end{pmatrix},$$

where $\cos\alpha = t_g \sin qa/(\omega - \epsilon)$. The eigenvalues of $\hat{X}$ are $x_{1,2} = -t_g \cos qa \pm \sqrt{(\omega-\epsilon)^2 - t_g^2 \sin^2 qa}$. We thus get

$$\hat{g}(q,\omega) = \begin{pmatrix} g & f \\ f' & g \end{pmatrix} = \frac{1}{t_g} \hat{U}\hat{R}_1\hat{R}_2 \begin{pmatrix} e^{i\phi_1} & 0 \\ 0 & e^{-i\phi_2} \end{pmatrix} \hat{R}_2^{-1}\hat{R}_1^{\dagger} = \frac{1}{2t_g \sin\alpha} \begin{pmatrix} e^{i\phi_1} - e^{-i\phi_2} & ie^{iqa}[e^{-i(\alpha-\phi_1)} - e^{i(\alpha-\phi_2)}] \\ -ie^{-iqa}[e^{i(\alpha+\phi_1)} - e^{-i(\alpha+\phi_2)}] & e^{i\phi_1} - e^{-i\phi_2} \end{pmatrix}, \quad (1)$$

where $\cos\phi_{1,2} = x_{1,2}/(2t_g)$. The eigenvalues $e^{i\phi_1}$ and $e^{-i\phi_2}$ have been chosen so that the resulting Green functions have the proper behavior when the frequency goes to infinity.

B. Finite graphene layer

Starting from the results of Sec. II A, one can obtain the Green's functions of a finite graphene layer by introducing a

perturbation consisting in breaking the bond between the Nth line and its neighbors on the $N+1$ line. From Dyson's equation, we obtain the following set of coupled equations:

$$\hat{g}^F_{n,n} = \hat{g}_{n,n} - \hat{g}_{n,N+1}\hat{t}\hat{g}^F_{N,n},$$

$$\hat{g}^F_{N,n} = \hat{g}_{N,n} - \hat{g}_{N,N+1}\hat{t}\hat{g}^F_{N,n}, \tag{2}$$

where the superindex F stands for the finite system and the subindices i,j indicate the lines within the layer. On the other hand, the elements $\hat{g}_{N,N+1}$ can be expressed as $\hat{g}_{N,N+1} = \hat{g}^F_{N,N}\hat{t}\hat{g}_{N+1,N+1}$. We now use $\hat{g}_{1,1} = \hat{g}$ and $\hat{g}_{n,N} = \hat{g}_{N,n} = (\hat{g}\hat{t})^{N-n}\hat{g}_{n,n}$, where $\hat{g}$ corresponds to the surface Green's function for the semi-infinite system derived in the previous section. Also, we have $\hat{g}_{N+1,N+1} = [\hat{g} - \hat{t}\hat{g}^F_{N,N}\hat{t}]^{-1}$ and $\hat{g}_{n,n} = [\hat{I} - (\hat{g}\hat{t})^{2n}][\hat{I} - (\hat{g}\hat{t})^2]^{-1}\hat{g}$, which allows to obtain

$$\hat{g}^F_{n,n} = [\hat{I} - (\hat{g}\hat{t})^2]^{-1}[\hat{I} - (\hat{g}\hat{t})^{2(N+1)}]^{-1}[\hat{I} - (\hat{g}\hat{t})^{2n}] \times [\hat{I} - (\hat{g}\hat{t})^{2(N-n+1)}]\hat{g},$$

$$\hat{g}^F_{n,N} = [\hat{I} - (\hat{g}\hat{t})^{2(N+1)}]^{-1}[\hat{I} - (\hat{g}\hat{t})^{2n}](\hat{g}\hat{t})^{N-n}\hat{g}. \tag{3}$$

By making use of the rotation matrix defined in Sec. II A, these quantities can be written in the following rather simple form:

$$\hat{g}^F_{n,n} = \frac{1}{t_g}\hat{R}\begin{pmatrix} \dfrac{\sin n\phi_1}{\sin\phi_1}\dfrac{\sin(N-n+1)\phi_1}{\sin(N+1)\phi_1} & 0 \\ 0 & \dfrac{\sin n\phi_2}{\sin\phi_2}\dfrac{\sin(N-n+1)\phi_2}{\sin(N+1)\phi_2} \end{pmatrix}\hat{R}^{-1}\hat{U},$$

$$\hat{g}^F_{n,N} = \frac{1}{t_g}\hat{R}\begin{pmatrix} \dfrac{\sin n\phi_1}{\sin(N+1)\phi_1} & 0 \\ 0 & \dfrac{\sin n\phi_2}{\sin(N+1)\phi_2} \end{pmatrix}\hat{R}^{-1}\hat{U}. \tag{4}$$

One can have the expression for the borders of the layer setting $n=1$ or $n=N$. Then, the eigenvalues of the Green's functions become $\sin N\phi_i/\sin(N+1)\phi_i$ and $\sin\phi_i/\sin(N+1)\phi_i$, with $i=1,2$, for the $\hat{g}^F_{1,1} = \hat{g}^F_{N,N}$ and $\hat{g}^F_{1,N} = \hat{g}^F_{N,1}$ cases, respectively. These expressions are equivalent to those for a finite tight-binding chain.[16]

The poles of these Green's functions determine the spectral properties of the layer. These poles are fixed by the condition $\sin(N+1)\phi_{1,2}=0$, which is satisfied by $\phi_{1,2} = m\pi/(N+1)$, where m is an integer. One can associate this condition with the quantization of the transverse momentum, which is used in the continuous model for describing armchair nanoribbons.[13] At the charge neutrality condition, the existence of zero energy states requires $\phi_{1,2} = \pm 2\pi/3$, which can only be satisfied for $N=3p+2$ (in a more compact notation for $N \bmod 3 = 2$). Therefore, the layers can be classified into metallic, for the $N \bmod 3 = 2$ case, and insulating, for the other cases ($N \bmod 3 = 0,1$). In the insulating cases, the gap in the spectrum is $2E_g$, where $E_g \simeq \pi\hbar v_F/3L$, with $L = Na/\sqrt{3}$ as the length of the layer. It should be noted that electron states in the metallic case are doubly degenerate, while the degeneracy is removed in the insulating cases.[13]

III. MODELING THE GRAPHENE-SUPERCONDUCTOR INTERFACE

One of the aims of the present work is to analyze different ways to describe the interface between a graphene layer and a superconductor. In the recent literature, it has been assumed that a superconducting electrode deposited on top of graphene induces a finite pairing amplitude and introduces a finite level of doping, which shifts the Fermi level of the graphene layer far away from the Dirac point.[3,4] This heavily doped superconducting graphene (HDSC) model provides a simple boundary condition for the effective Dirac–Bogoliubov–de Gennes equations describing the interface.

One can alternatively imagine that the graphene layer is directly coupled to a bulk superconducting electrode by means of a sharp interface, which breaks the coherence between the two graphene sublattices. We shall refer to this case as the bulk-BCS model. We wish to analyze the differences between the two models, which are schematically represented in Fig. 2.

The presence of superconducting correlations requires introducing the Nambu space, describing electron and hole propagation within the graphene layer. All Green's functions acquire a 2×2 structure in Nambu space. For the uncoupled graphene, we have

$$\check{\hat{g}} = \begin{pmatrix} \hat{g}_e & 0 \\ 0 & \hat{g}_h \end{pmatrix}, \tag{5}$$

where $\hat{g}_e$ corresponds to the propagators obtained in Sec. II and $\hat{g}_h$ is obtained from $\hat{g}_e$ by changing $\epsilon \to -\epsilon$ and $t_g \to -t_g$ (notice that we use the hat symbol to denote the sublattice space while the check symbol indicates the Nambu space).

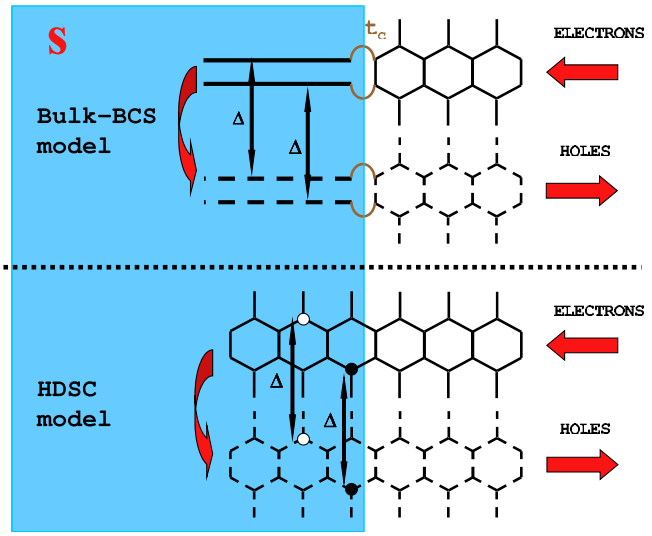

FIG. 2. (Color online) Schematic picture of an Andreev reflection in the bulk-BCS and in the HDSC models. In the first case, the sites on each sublattice of the graphene edge are coupled to the superconductor through independent channels, thus breaking the coherence of the honeycomb structure. In the other case, the coupling with the superconducting region maintains this structure. The hopping element t_c in the bulk-BCS model controls the normal transparency of the interface. The vertical arrows represent the coupling between electrons and holes in Nambu space given by the gap parameter Δ.

The effect of the coupling with the superconducting electrode can be introduced by means of a self-energy $\check{\Sigma}$, which renormalizes the uncoupled Green's functions. Thus, the local Green's function on the graphene edge at the interface is determined by $[\check{g}^{-1}-\check{\Sigma}]^{-1}$.

In the case of the bulk-BCS model, the self-energy is momentum independent and does not have a structure in the sublattice space; i.e.,

$$\check{\Sigma} = \pi\rho_s t_c^2 \check{\tau}_z \check{g}_{BCS} \check{\tau}_z \otimes \hat{I}, \tag{6}$$

where $\check{\tau}_z$ is the z Pauli matrix in Nambu space and t_c^2 is the mean square hopping element between the graphene layer and the superconducting electrode. This quantity controls the value of the parameter $\beta = t_c^2 \pi\rho_s / t_g$, which characterizes the quality of the interface, where ρ_s is the DOS. On the other hand, $\check{g}_{BCS} = g_s \check{I} + f_s \check{\tau}_x$ stands for the dimensionless BCS Green's function, i.e., $g_s = -\omega/\sqrt{\Delta^2-\omega^2}$ and $f_s = \Delta/\sqrt{\Delta^2-\omega^2}$.

We would like now to derive the expression of the self-energy within the HDSC model. We first notice that in the heavily doped limit, one has $|\epsilon| \gg |\omega|, t_g \sin qa$ for the relevant range of frequencies and q values. Thus, in $\hat{R}_2$, one has $\alpha \to \pi/2$. In the new basis, the system is equivalent to a tight-binding chain with site energies $\epsilon \pm t_g$ and local pairing fixed by Δ. Although the exact Green's functions for this system is rather complicated, for low energies, it can be approximated by

$$\hat{R}_2^{-1} \check{g} \hat{R}_2 \simeq \begin{pmatrix} \pi\rho_+ & 0 \\ 0 & \pi\rho_- \end{pmatrix} \otimes \check{g}_{BCS} + \frac{1}{2t_g^2} \begin{pmatrix} \epsilon + t_g & 0 \\ 0 & \epsilon - t_g \end{pmatrix} \otimes \check{\tau}_z, \tag{7}$$

where $\pi\rho_\pm = \sqrt{1-(\frac{\epsilon \pm t_g}{2t_g})^2}/t_g$. By further taking the approximation $|\epsilon| \ll t_g$ and transforming back into the site representation, we obtain the following self-energy:

$$\check{\Sigma}/t_g \simeq \frac{\sqrt{3}}{2} \check{\tau}_z \check{g}_{BCS} \check{\tau}_z \otimes \hat{I} - \frac{1}{2} \check{\tau}_z \otimes \hat{\sigma}_x. \tag{8}$$

Notice that, in contrast to the first model, the self-energy in the HDSC model does exhibit a structure in the sublattice space. However, it satisfies the condition $\det \check{\Sigma}/t_g = 1$. This structure turns out to be of importance in connection to Andreev reflection as discussed in the next section. In the following, we will use a general form of the model self-energies, which can be expressed as $\check{\Sigma} = \beta \check{\tau}_z \check{g}_{BCS} \check{\tau}_z \otimes \hat{I} - \gamma \check{\tau}_z \otimes \hat{\sigma}_x$. Thus, appropriate values for β and γ will correspond to the different models (i.e., $\gamma = 0$ with arbitrary β for the bulk-BCS model, while $\beta = \sqrt{3}/2$ and $\gamma = 1/2$ in units of t_g for the HDSC model).

IV. ANDREEV REFLECTION AT A GRAPHENE-SUPERCONDUCTOR INTERFACE

The Andreev reflection is the basic mechanism for the conversion of a quasiparticle current into a supercurrent at the interface between a normal metal and a superconductor. In the case of a graphene-superconductor interface like the one we have described in SecIII, there are two channels for the incident electrons with a given wave vector q corresponding to the states, which diagonalize the $\hat{X}$ matrix. The reflected hole can be in either of these two channels. Our microscopic theory can thus describe a more general situation than the idealized model for the interface used in Ref. 3, which assumes only one channel for the reflected hole for a given wave vector.

The Andreev reflection amplitudes can be expressed in terms of Green's functions. Generalizing previous works,[17,18] we can derive the expression

$$\hat{r}_A(q,\omega) = 2i\hat{A}_e^{1/2} \{\check{\Sigma}[\check{I} - \check{g}\check{\Sigma}]^{-1}\}_{eh} \hat{A}_h^{1/2}, \tag{9}$$

where $\hat{A}_{e,h}(q,\omega) = [\hat{g}_{e,h}(q,\omega) - \hat{g}_{e,h}^\dagger(q,\omega)]/2i$. Using the general form of the model self-energies discussed in Sec. III allows us to reduce the expression of $\hat{r}_A$ to

$$\hat{r}_A = 2i\hat{A}_e^{1/2} \beta f_s [\hat{I} - \beta g_s (\hat{g}_e + \hat{g}_h) - \gamma(\hat{g}_h \hat{\sigma}_x - \hat{\sigma}_x \hat{g}_e) - (\beta^2 + \gamma^2) \hat{g}_h \hat{g}_e]^{-1} \hat{A}_h^{1/2}. \tag{10}$$

This expression becomes particularly simple when $\epsilon = 0$ because $g^e = g^h$, $f^e = -f^h$, and $f'^e = -f'^h$. So, $\hat{r}_A$ is a scalar quantity given by

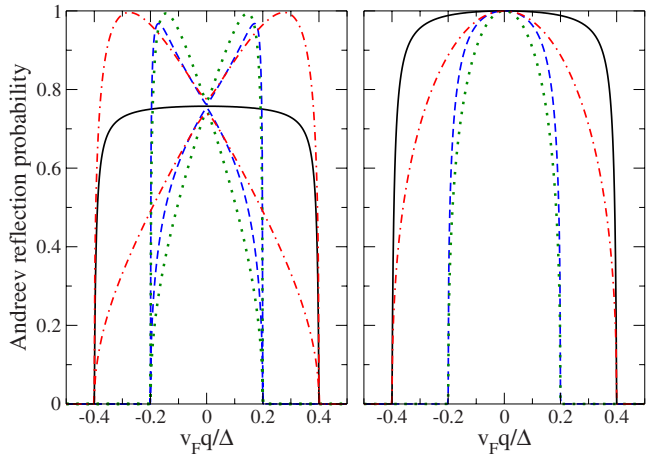

FIG. 3. (Color online) Andreev reflection probability on the two eigenchannels as a function of the parallel momentum q for fixed energy $\omega=0.2\Delta$. The left panel corresponds to the bulk-BCS model (with $\beta=1$) and the right one to the HDSC model. The different curves correspond to different values of the doping level ϵ: 0 (full lines), 0.1 (dashed lines), 0.3 (dotted lines), and 0.4Δ (dashed-dotted lines).

$$\hat{r}_A = \frac{4\beta f_s(\mathrm{Im}\, g^2 - |f - f'^*|^2)}{1 - \mathrm{Tr}[(\beta g_s \hat{I} \mp \gamma\hat{\sigma}_x)\hat{g}_{e,h}] - (\beta^2 + \gamma^2)\det \hat{g}_{e,h}}\hat{I}, \quad (11)$$

where $\mathrm{Tr}[(\beta g_s \hat{I} \mp \gamma\hat{\sigma}_x)\hat{g}_{e,h}] = [2\beta g_s g - \gamma(f+f')]$ and $\det \hat{g}_{e,h} = (g^2 - ff')$.

In general, doping conditions (i.e., when $\epsilon \neq 0$) $\hat{r}_A$ is not a scalar within the bulk-BCS model. The eigenvalues of $\hat{r}_A\hat{r}_A^\dagger$ give the Andreev reflection probability decomposed into two eigenchannels for each wave vector q. The evolution of these eigenvalues for fixed ω and increasing ε as a function of q is shown in the left panel of Fig. 3. Their maximum value is reached for $\beta=1$ and it never exceeds ~ 0.76 at normal incidence. Within the HDSC model, however, $\hat{r}_A$ remains scalar for arbitrary doping and it always reaches the unitary limit at $q=0$ (see right panel of Fig. 3).

It is also interesting to analyze the physical character of the Andreev reflection in the two models. The information on how the eigenchannels of the uncoupled structure are connected by an Andreev process is contained in the matrix $\hat{R}_e\hat{r}_A\hat{R}_h^{-1}$. As $\hat{r}_A$ is a scalar within the HDSC model, the channel mixing is determined by $\hat{R}_e\hat{R}_h^{-1}$. This is also the case for the bulk-BCS model at zero doping. In this case, we have $\alpha_h = \pi - \alpha_e$ and thus electrons injected in one channel emerge as holes in the opposite one. The momentum in the y direction is conserved in this process, and therefore, this type of reflection corresponds to what has been described in Ref. 3 as *specular Andreev reflection*. On the other hand, for $\epsilon \neq 0$ and $\omega \to 0$, we have $\alpha_h = \alpha_e$, which corresponds to the usual (retro)reflection where holes are reflected on the same channel as the incident electron. For intermediate doping situations, both types of reflection would be present although with a dominance of specular (retro)reflection for $\omega > \epsilon$ ($\omega < \epsilon$).

To complete the analysis in this section, we have computed the differential conductance per unit length due to Andreev processes, which is given by[19]

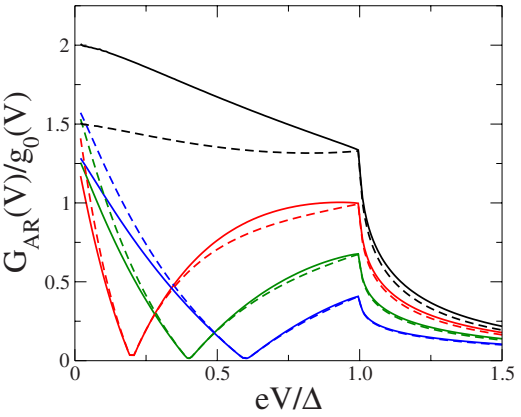

FIG. 4. (Color online) Total differential conductance per unit length due to Andreev reflection G_{AR} normalized to the conductance per unit length of a ballistic graphene layer $g_0(V) = \frac{4e^2}{h}(eV + \epsilon)/(\pi\hbar v_F)$. The results for the HDCS model (full lines) and for the bulk-BCS model (dashed lines) are compared with increasing doping level $\epsilon = 0$, 0.2, 0.4, and 0.6Δ.

$$G_{AR} = \frac{2e^2}{h}\frac{1}{2\pi}\int_{-\pi/a}^{\pi/a} dq\, \mathrm{Tr}[\hat{r}(q,eV)\hat{r}^\dagger(q,eV)]. \quad (12)$$

The results for G_{AR} within the two models are shown in Fig. 4. As suggested in Ref. 3, we normalize the result by the conductance per unit length of a ballistic graphene sheet, which in the low energy limit is given by $g_0(V) = \frac{4e^2}{h}(eV + \epsilon)/(\pi\hbar v_F)$. As can be observed, at the charge neutrality point, the HCSD model yields a maximum of ratio $G_{AR}/g_0 = 2$ at zero voltage, dropping to ~ 1.33 for $\epsilon > 0$, which is in agreement with the results of Ref. 3. This ratio is of the order of ~ 1.63 in the bulk-BCS model with $\beta=1$ regardless of the doping level. The qualitative behavior of the differential conductance with ϵ is similar in both models and agrees with the results of Ref. 3.

V. PROXIMITY EFFECT ON A FINITE GRAPHENE LAYER

By using the previous results, one can analyze the effect of the coupling with the superconductor on the spectral properties of a graphene layer of finite size. Again, we will focus on the differences between the bulk-BCS and the HDSC models for the interface. From Dyson's equation, it is straightforward to obtain the Green's functions at the edge of the layer (labeled as 1) when the coupling to the superconductor is introduced on the opposite edge (labeled as N). Then, for an arbitrary line n inside the layer, we have

$$\check{\hat{G}}_{n,n} = \check{\hat{g}}^F_{n,n} + \check{\hat{g}}^F_{n,N}\check{\hat{\Sigma}}[\hat{I} - \check{\hat{g}}^F_{N,N}\check{\hat{\Sigma}}]^{-1}\check{\hat{g}}^F_{N,n}, \quad (13)$$

where $\check{\hat{\Sigma}}$ stands for the general form of the self-energy introduced in Sec. III. We can further reduce this expression to

$$\overset{\times}{\hat{G}}_{n,n} = \overset{\times}{g}{}^{F}_{n,n} + \overset{\times}{g}{}^{F}_{n,N} \begin{pmatrix} [\beta g_s - \gamma\hat{\sigma}_x + (\beta^2+\gamma^2)\hat{g}^{Fh}_{N,N}]\hat{D}_e^{-1} & -\beta f_s \hat{D}_h^{-1} \\ -\beta f_s \hat{D}_e^{-1} & [\beta g_s + \gamma\hat{\sigma}_x + (\beta^2+\gamma^2)\hat{g}^{Fe}_{N,N}]\hat{D}_h^{-1} \end{pmatrix} \overset{\times}{g}{}^{F}_{N,n}. \tag{14}$$

The quantities $\hat{D}_e$ and $\hat{D}_h$ have the following general form, which is expressed in the graphene subspace:

$$\hat{D}_e = \hat{I} - \beta g_s(\hat{g}^F_e + \hat{g}^F_h) - \gamma(\hat{g}^F_e\hat{\sigma}_x - \hat{\sigma}_x\hat{g}^F_h) - (\beta^2+\gamma^2)\hat{g}^F_e\hat{g}^F_h, \quad \hat{D}_h = \hat{I} - \beta g_s(\hat{g}^F_e + \hat{g}^F_h) - \gamma(\hat{g}^F_h\hat{\sigma}_x - \hat{\sigma}_x\hat{g}^F_e) - (\beta^2+\gamma^2)\hat{g}^F_h\hat{g}^F_e.$$

As in SecIV, in the limit where $\varepsilon=0$, these two denominators become equal and simplify to a scalar D because $\beta g_s(\hat{g}^F_e+\hat{g}^F_h)+\gamma(\hat{g}^F_e\hat{\sigma}_x-\hat{\sigma}_x\hat{g}^F_h)=\mathrm{Tr}[(\beta g_s\hat{I}\mp\gamma\hat{\sigma}_x)\hat{g}^F_{e,h}]$ and $\hat{g}^F_e\hat{g}^F_h=\det\hat{g}^F$. Then,

$$D = 1 - \mathrm{Tr}[(\beta g_s\hat{I}\mp\gamma\hat{\sigma}_x)\hat{g}^F_{e,h}] - (\beta^2+\gamma^2)\det\hat{g}^F_{e,h} \tag{15}$$

By using the expression of the finite layer Green's functions given in Sec. II and the rotation given in Sec. I, one can easily show that

$$\det[\hat{g}^F_{e,h}] = -\frac{1}{t_g^2}\frac{\sin(N\phi_1)\sin(N\phi_2)}{\sin[(N+1)\phi_1]\sin[(N+1)\phi_2]},$$

$$\mathrm{Tr}[(\beta g_s\hat{I}\mp\gamma\hat{\sigma}_x)\hat{g}^F_{e,h}] = \frac{1}{t_g\sin\alpha}\left\{\frac{\sin(N\phi_1)\sin[(N+1)\phi_2][\beta g_s-\gamma\sin(\alpha+q)]}{\sin[(N+1)\phi_1]\sin[(N+1)\phi_2]} - \frac{\sin(N\phi_2)\sin[(N+1)\phi_1][\beta g_s+\gamma\sin(\alpha-q)]}{\sin[(N+1)\phi_1]\sin[(N+1)\phi_2]}\right\}.$$

The zeroes of D determine the poles of the coupled system Green's functions. From them, one can thus analyze the distortion of the spectrum due to the superconducting proximity effect. For the charge neutrality case, these zeroes can be obtained from

$$\frac{-\beta\omega^2}{\sqrt{\omega^2 - t_g^2\sin^2 qa}\sqrt{\Delta^2-\omega^2}} = \frac{\sin[(N+1)\phi_1]\sin[(N+1)\phi_2] + (\beta^2+\gamma^2)\sin(N\phi_1)\sin(N\phi_2)}{\sin(N\phi_1)\sin[(N+1)\phi_2] - \sin(N\phi_2)\sin[(N+1)\phi_1]} + \frac{\gamma}{\sin\alpha}\frac{\sin(\alpha+q)\sin(N\phi_1)\sin[(N+1)\phi_2] + \sin(\alpha-q)\sin(N\phi_2)\sin[(N+1)\phi_1]}{\sin(N\phi_1)\sin[(N+1)\phi_2] - \sin(N\phi_2)\sin[(N+1)\phi_1]}. \tag{16}$$

The spectrum corresponds to a series of subbands, which quadratically disperse as a function of q in the small q limit. As in the uncoupled case, the precise form of the dispersion relation depends on the value of N mod 3. In the case where the uncoupled layer is metallic (N mod 3=2), the coupling to the superconductor induces a *minigap* in the lowest band. The existence of this minigap in the spectrum is similar to what is found for diffusive conductors and can be associated with the pseudodiffusive behavior of graphene at the charge neutrality point.[14,15] For the cases N mod 3=0,1, the uncoupled layer is insulating and the coupling of the superconductor just leads to a renormalization of the gap in the spectrum. We shall denote by E_g^* the lowest energy level for all three cases.

The dependence E_g^* as a function of N and the interface parameters β and γ can be obtained from Eq. (16) with $q=0$. For large N, this level decreases as $1/N$ with a prefactor, which depends on N mod 3 and the interface parameters. Figure 5 describes the behavior of E_g^* both in the bulk-BCS and in the HDSC models. The left panel shows the lowest energy state within the bulk-BCS model as a function of the interface transparency parameter (β) for fixed N. The three cases N mod 3=0,1,2 are shown. As can be observed, in the metallic case, the minigap evolves from zero at $\beta=0$ to a maximum value at $\beta=1$. On the other hand, the two insulating cases exhibit different behavior. While the starting value at $\beta=0$ is fixed by E_g in both cases, in the case N mod 3 =0, it decreases until it reaches the same value as the one of the N mod 3=2 case for $\beta=1$. hand, E_g^* remains approximately constant for N mod 3=1. This behavior indicates that the proximity effect is almost negligible in this case. The right panel shows the behavior of the lowest energy state as a function of N both in the bulk-BCS model with $\beta=1$ and in the HDSC. The results are universal (i.e., independent of the ratio Δ/t_g) when plotted as a function of L/ξ, where $\xi=\hbar v_F/\pi\Delta$ is the superconducting coherence length. It is interesting to note that while in the bulk-BCS model, two limiting $1/L$ curves, corresponding to N mod 3=0,2 and N mod 3=1, appear; in the HDSC model, E_g^* lay on the same $1/L$ curve regardless of N (dashed line in Fig. 5).

A. Local density of states

We define the electronic LDOS on a line n within the graphene layer as

$$\rho_n(\omega) = \frac{a}{(2\pi)^2}\int_{-\frac{\pi}{a}}^{\frac{\pi}{a}} dq\ \mathrm{Tr}\,\mathrm{Im}[\hat{G}_{n,n}(q,\omega)], \tag{17}$$

which has been normalized to one electron per site and spin. The LDOS thus defined is measured in units of $a/\hbar v_F$. How-

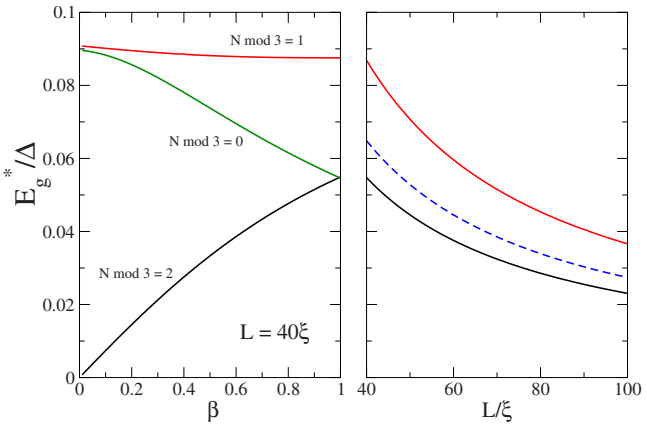

FIG. 5. (Color online) Evolution of the lowest energy level E_g^* of a finite graphene layer coupled to a superconductor as a function of β within the bulk-BCS model for $L=40\xi$ (left panel) and with the length of the layer L within both the bulk-BCS (at $\beta=1$) and the HDSC models (right panel). In the case of the bulk-BCS model for arbitrary β, three different behaviors are found depending on the N mod 3 value. On the contrary, a universal behavior of E_g^* is found within the HDSC model regardless of the N value (see text).

ever, to study the proximity effect, it is more convenient to normalize the LDOS with the density of a bulk graphene layer with zero doping at $\omega=\Delta$, ρ_0, which for $\Delta \ll \hbar v_F/a$ is given by $\Delta/2\pi(a/\hbar v_F)^2$. The results thus obtained do not depend on the choice of the ratio Δ/t_g used in our tight-binding calculations.

The LDOS on a metallic layer (N mod 3=2) is shown in Fig. 6. The results for the coupled case within the HDCS model are compared to the results for the uncoupled case. It is typically found that the number of singularities in the LDOS (associated with the number of subbands) in a given energy interval is doubled as compared to the uncoupled case. This effect is due to the breaking of the double degeneracy of the bands due to the coupling with the superconductor. The LDOS also exhibits an oscillatory behavior with the position on the layer. This behavior reflects the properties of the electronic wave functions and, as in the case of isolated nanoribbons,[13] is distinct for lines with n mod 3=1,2 and lines with n mod 3=0. We thus illustrate these cases separately on the top and on the lower panels of Fig. 6.

The right panels of Fig. 6 show the evolution along the layer of the LDOS close to the singularities. We illustrate this evolution at three different energies corresponding to the lowest first singularities, indicated by $m=0,1$ and 2 in Fig. 6. For reference, we also show the spatial variation of the LDOS close to the first singularity for the uncoupled case. In this case, the LDOS reaches a maximum value at the edges of the layer and a minimum in the middle for lines n mod 3=1,2, while the opposite behavior is found for n mod 3=0. In the coupled case, one can still identify the singularities with the oscillation pattern in the LDOS but it no longer reaches an extreme value at the edge of the layer in contact with the superconductor.

As a final remark, we note that in the case of insulating nanoribbons, the coupling to the superconductor just induces a shift singularities in the spectrum but do not change their number. This is due to the nondegenerate character of the bands of the uncoupled layer.

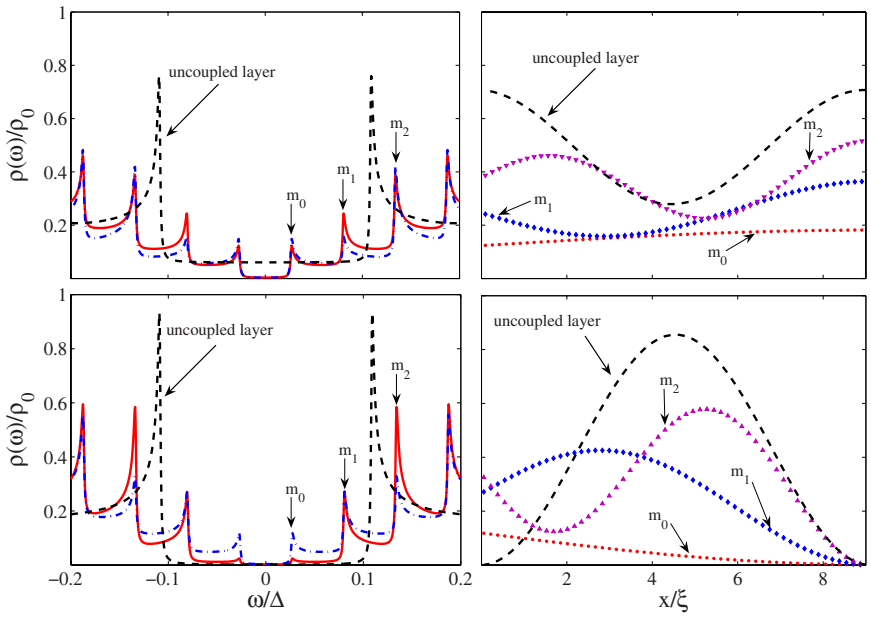

FIG. 6. (Color online) Spatial variation of the LDOS on a finite layer ($L=9\xi$) in the HDSC model. The plots on the top panels correspond to the lines inside the layer with n mod 3=1,2 and those on lower ones correspond to n mod 3=0. The uncoupled layer has a metallic behavior (N mod 3=2). The LDOS for this case, at the edges of the layer (top left panel) and at the center of the layer (lower left panel), is plotted with dashed lines. When coupled to the superconductor, the LDOS is modified by the appearance of a minigap (denoted as m_0 in the pictures) and with the breaking of the uncoupled bands into a pair of sub-bands (m_1 and m_2 in the pictures). The evolution of the LDOS along the layer is shown in the right panels. The results are normalized to the LDOS of a bulk graphene layer with zero doping at $\omega=\Delta$, denoted by ρ_0.

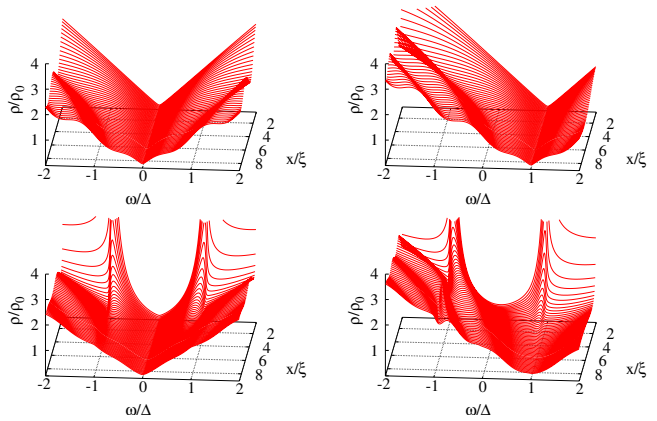

FIG. 7. (Color online) LDOS on lines of type n mod 3=1 for a semi-infinite graphene layer coupled to a superconductor within the bulk-BCS model (lower panels). The upper panels show the corresponding results for the uncoupled case. The plots on the left correspond to the undoped case while those on the right correspond to $\epsilon=\Delta$.

VI. PROXIMITY EFFECT ON A SEMI-INFINITE GRAPHENE LAYER

The results of Sec. V can be extended to analyze the spectral properties of a semi-infinite graphene layer coupled to a superconductor. The local Green's function on a line n is given by

$$\check{g}_{n,n} = [\check{G}_{n,n}^{-1} - t_g^2 \check{g}]^{-1},$$

where $\check{G}_{n,n}$ is the Green's function for a finite graphene layer coupled to a semi-infinite superconducting layer obtained in the previous section and $\check{g}$ is the Green's function for the edge of the semi-infinite layer.

Figure 7 illustrates the spatial variation of the LDOS on a semi-infinite graphene layer and the effect of varying the doping level within the bulk-BCS model. For reference, we show the LDOS for the uncoupled case on the upper panels. As can be observed, the uncoupled LDOS exhibits long wavelength oscillations on the $\sim \hbar v_F/|\omega|$ scale on top of the characteristic V shape behavior. These oscillations are a surface effect, which decreases in amplitude inside the layer, as shown in Fig. 8, where the LDOS profile at $\omega=2\Delta$ is plotted on a larger scale. A similar effect has been shown to occur in the case of nanoribbons with zigzag edges.[20]

The superconducting proximity effect is manifested by the appearance of sharp peaks in the LDOS for energies $|\omega| \sim \Delta$ (lower panels in Fig. 7). These peaks distort the V shape density of states (DOS), an effect which decays within a few times the coherence length inside the layer. The small oscillations on the $\hbar v_F/|\omega|$ scale are reduced compared to the uncoupled case but are still observable within the bulk-BCS model (indicated by the full line in Fig. 8).

The overall behavior of the LDOS within the HDSC model is very similar although in this last case, the $\hbar v_F/|\omega|$ oscillations are further suppressed (dashed line in Fig. 8).

The right panels in Fig. 7 illustrate the effect on the LDOS of a displacement from the charge neutrality condition

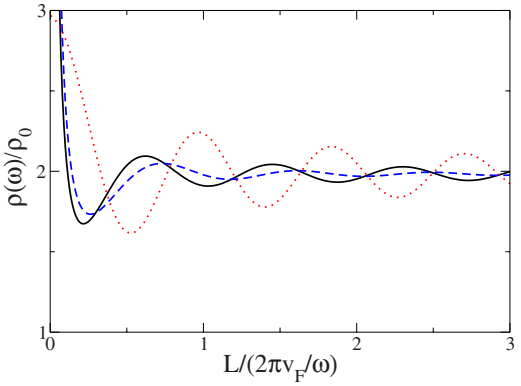

FIG. 8. (Color online) Oscillation pattern on the LDOS of a semi-infinite graphene layer at zero doping within the bulk-BCS model (full line), the HDCS model (dashed line), and in the uncoupled case (dotted line). The energy is fixed at $\omega=2\Delta$.

by applying a gate potential (finite ε). It is observed that the V shape is essentially rigidly displaced while the peaks induced by the proximity effect remain fixed at $\omega \sim \pm\Delta$. hand, the wavelength of the oscillation pattern is, in this case, set by $\hbar v_F/|\omega-\varepsilon|$.

VII. CONCLUSIONS

We have presented a theoretical analysis of the proximity effect at a graphene-superconductor interface. For this study, we have first derived analytical expressions for the Green's functions on an armchair edge of a semi-infinite graphene layer and for a finite layer.

Two models for microscopically describing the coupling to a superconductor have been presented. In the first model, a bulk superconducting electrode is directly connected to the armchair edge of a graphene sheet (bulk-BCS model). The honeycomb structure of graphene is broken and this is reflected in the different behavior of the Andreev reflection probability on the two eigenchannels of the graphene sheet as a function of the parallel momentum q. Only for the case of zero doping both eigenchannels are equivalent. Within this model, one can study the effect of varying the normal transparency of the interface (through parameter β). The Andreev reflection probability at normal incidence never reaches unity within this model but has a maximum value of $\sim$0.76. In the second model, it is assumed that the superconducting electrode induces a finite order parameter on the graphene regions underneath. This model thus maintains the graphene sublattice structure and, as we have shown, the Andreev reflection amplitude $\hat{r}_A(q,\omega)$ is a scalar quantity for arbitrary doping and always reaches the unitary limit for normal incidence.

We have also studied the effect of the coupling to the superconductor on the spectral properties of finite and semi-infinite graphene layers. For finite layers, we have obtained a simple expression for the energy spectrum of the coupled system, which can be numerically evaluated easily. We have shown that a metallic ribbon develops a minigap whose size inversely decreases with the length of the layer. This effect can be associated with the pseudodiffusive behavior of

graphene. The induced minigap is slightly smaller in the bulk-BCS model with $\beta=1$ than in the HDSC model.

For the semi-infinite case, the proximity effect manifests in the appearance of peaks in the DOS for frequencies $|\omega| \sim \Delta$. These peaks rapidly decay inside the graphene sheet for distances a few times the superconducting coherence length ξ. hand, the LDOS keeps its characteristic V shape for zero doping for frequencies $|\omega| < \Delta$. We expect that these findings can be useful to analyze future scanning tunneling microscopy experiments on graphene sheets with superconducting electrodes.

ACKNOWLEDGMENTS

This work has been financed by the Spanish CYCIT (Contract No. FIS2005-06255). Discussions with J.C. Cuevas, L. Brey, and H. Le Sueur are acknowledged.

[1] K. Novoselov, A. K. Geim, S. V. Morozov, D. Jang, Y. Zhang, S. V. Dubonos, I. V. Grigorieva, and A. A. Firsov, Science **306**, 666 (2004).
[2] W. H. Matthaeus, J. J. Ambrosiano, and M. L. Goldstein, Phys. Rev. Lett. **53**, 1449 (1984); D. P. DiVincenzo and E. J. Mele, Phys. Rev. B **29**, 1685 (1984); T. Ando, T. Nakanishi, and R. Saito, J. Phys. Soc. Jpn. **67**, 2857 (1998); V. P. Gusynin and S. G. Sharapov, Phys. Rev. Lett. **95**, 146801 (2005).
[3] C. W. J. Beenakker, Phys. Rev. Lett. **97**, 067007 (2006).
[4] M. Titov and C. W. J. Beenakker, Phys. Rev. B **74**, 041401(R) (2006).
[5] Ali G. Moghaddam and M. Zareyan, Phys. Rev. B **74**, 241403(R) (2006).
[6] A. Ossipov, M. Titov, and C. W. J. Beenakker, Phys. Rev. B **75**, 241401(R) (2007).
[7] J. C. Cuevas and A. L. Yeyati, Phys. Rev. B **74**, 180501(R) (2006).
[8] H. B. Heersche, P. Jarillo-Herrero, J. B. Oostinga, L. M. K. Vandersypen, and A. Morpurgo, Nature (London) **446**, 56 (2007); H. B. Heersche, P. Jarillo-Herrero, J. B. Oostinga, L. M. K. Vandersypen, and A. Morpurgo, Solid State Commun. **143**, 72 (2007); A. Shailos, W. Nativel, A. Kasumov, C. Collet, M. Ferrier, S. Gueron, R. Deblock, and H. Bouchiat, Europhys. Lett. **79**, 57008 (2007); F. Miao, S. Wijeratne, Y. Zhang, U. C. Coskun, W. Bao, and C. N. Lau, Science **317**, 1530 (2007).
[9] H. Le Sueur (private communication).
[10] M. Titov, A. Ossipov, and C. W. J. Beenakker, Phys. Rev. B **75**, 045417 (2007).
[11] H. Schomerus, Phys. Rev. B **76**, 045433 (2007); Y. M. Blanter and I. Martin, *ibid.* **76**, 155433 (2007).
[12] The fabrication of graphene nanoribbons with well defined edges at the atomic scale has been recently reported; see X. Li, X. Wang, L. Zhang, S. Lee, and H. Dai, Science **319**, 1229 (2008).
[13] L. Brey and H. A. Fertig, Phys. Rev. B **73**, 235411 (2006).
[14] A. R. Akhmerov and C. W. J. Beenakker, Phys. Rev. B **75**, 045426 (2007).
[15] E. Prada, P. San-Jose, B. Wunsch, and F. Guinea, Phys. Rev. B **75**, 113407 (2007).
[16] E. Vecino, A. Martín-Rodero, and A. Levy Yeyati, Phys. Rev. B **64**, 184502 (2001).
[17] J. C. Cuevas, A. Martín-Rodero, and A. L. Yeyati, Phys. Rev. B **54**, 7366 (1996).
[18] J. C. Cuevas, A. L. Yeyati, and A. Martín-Rodero, Phys. Rev. Lett. **80**, 1066 (1998).
[19] G. E. Blonder, M. Tinkham, and T. M. Klapwijk, Phys. Rev. B **25**, 4515 (1982).
[20] G. Tkachov, Phys. Rev. B **76**, 235409 (2007).